Theoretical and experimental study of opposite lateral shifts and polarization beam splitting on symmetrical metal-cladding waveguides

Lin Chen, Yiming Zhu, Yan Peng and Songlin Zhuang

Shanghai Key Laboratory of Modern Optical System, College of Optics and Electronic Information Engineering, University of Shanghai for Science and Technology, 516 JunGong Road, Shanghai 200093, People's Republic of China

E-mail: ymzhu@usst.edu.cn and linchen@usst.edu.cn

Abstract
Simultaneously opposite lateral shifts and polarization beam splitting are demonstrated theoretically and experimentally when reflection occurs on a symmetrical metal-cladding waveguide (SMCW). It was investigated that, at large incident angle, TE and TM polarized incident beams experience opposite lateral shifts simultaneously, which can be enhanced to hundreds of micrometers. This is due to the strong mode dispersion on the SMCW when the low order mode is excited. Experimental results have demonstrated the above theoretical results obtained by using the stationary phase method and the Gaussian beam model. This phenomenon has potential applications in optical devices.

Keywords: symmetrical metal-cladding waveguide, Goos–Hänchen effect, polarization beam splitting

(Some figures in this article are in colour only in the electronic version)

1. Introduction

The Goos–Hänchen (GH) effect, which refers to beam position lateral shifts when a light beam totally reflects from a boundary between two semi-infinite dielectric media, was first experimentally demonstrated by Goos and Hänchen [1, 2]. In the case of a structure with two layers, the GH shift is of the order of the incident wavelength. Various structures and materials have been proposed to enlarge the GH shift [3–9]. Recently, it was recognized that a enhanced GH shift coming from a light beam reflected through a weakly absorbing dielectric slab can be one order larger than the wavelength of light [6]. Furthermore, beam shifts reflected from symmetrical metal-cladding waveguide (SMCW) structures can also be extremely enhanced [7], which comes from transfer of the energy from the incident wave. The GH effect of SMCWs has wide applications in refractive index (RI) sensors [10], displacement sensors [11], superprisms [12] and electric control of spatial beam position [13]. In addition,

large and opposite GH shifts for transverse electric (TE) and transverse magnetic (TM) polarizations were predicted simultaneously from a double-prism configuration [8] and at a interface associated with single-negative materials [9]. This interesting phenomenon can be used to achieve spatial polarization deviation and may lead to potential applications for characterizing the permittivity ε and permeability μ of materials [9].

In this work, we theoretically and experimentally demonstrate that enhanced and opposite lateral shifts for TE and TM polarizations reflected from SMCWs occur at same time. From the simulated and experimental results, we can obtain that GH shifts for TE and TM polarizations could separate from each other effectively when the incident angle of the light beam for the exciting low order mode in SMCWs is large enough. When the thickness of the upper metal layer h is larger than the critical thickness h_{cr} a negative shift can be observed; and conversely a positive shift occurs when $h < h_{cr}$. The critical thickness of the upper metal layer, h_{cr}, for TM
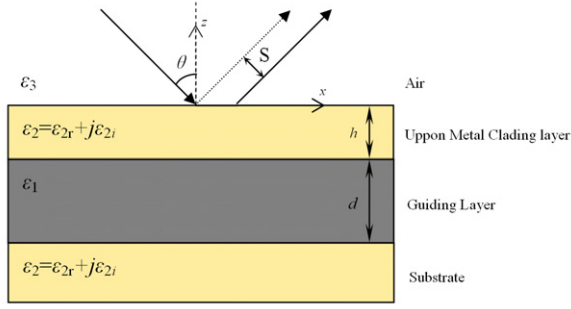
Figure 1. GH effect in the SMCW structure.

polarization is much larger than that for TE polarization. If the thickness of the upper metal layer, h, is selected to be larger than h_{cr} for TE polarization and less than h_{cr} for TM polarization, the opposite shifts for TE and TM polarizations can be obtained at the same time. Such kinds of opposite GH shifts can reach hundreds of micrometers experimentally with $h = 22$ nm at the incident wavelength 859.031 nm. The profiles of reflected TE and TM polarized beams were also observed to verify the polarization beam splitting effect by using a Gaussian model.

2. Theory

The structure of the SMCW is illustrated in figure 1. A dielectric slab with submillimeter scale (thickness d, dielectric constant ε_1) is sandwiched between two metal films. The upper metal layer (thickness h, dielectric constant ε_2) is a coupling layer and the bottom metal layer (dielectric constant ε_2) serves as both a substrate and reflecting panel. When a laser beam is cast on the upper layer by free space coupling, a large part of the energy couples into the guiding layer, which results in an attenuated total reflection dip. Additionally, by adjusting the incident wavelength, the components of wavevector along the propagation direction can coincide with the propagation constant of the guided wave exactly. Under such conditions, the GH shift can be enhanced dramatically. The origin of this phenomenon is because the energy of the guided wave is strongly confined in the guiding layer of the SMCW [14].

By employing the Fresnel formulae, the reflection coefficient of the SMCW can be written as

$$r = e^{-i\phi_{32}}$$
$$\times \frac{[1 - e^{i2(\kappa_1 d - \phi_{12})}] + [e^{i2(\kappa_1 d - \phi_{12})} - e^{-i2\phi_{12}}]e^{i\phi_{32}}e^{-2p_2h}}{[1 - e^{i2(\kappa_1 d - \phi_{12})}] + [e^{i2(\kappa_1 d - \phi_{12})} - e^{-i2\phi_{12}}]e^{-i\phi_{32}}e^{-2p_2h}}$$
(1)

where ϕ_{ij} is the phase difference between the media i and j. ϕ_{ij} can be described as

$$\phi_{ij} = \begin{cases} \arctan\left(\dfrac{p_j}{\kappa_i}\right) & \text{TE polarization} \\ \arctan\left(\dfrac{\varepsilon_i}{\varepsilon_j}\dfrac{p_j}{\kappa_i}\right) & \text{TM polarization,} \end{cases}$$
(2)

where $\kappa_i = (k_0^2\varepsilon_i - \beta^2)^{1/2}$ and $p_i = (\beta^2 - k_0^2\varepsilon_i)^{1/2}$ are the normal components of the wavevector in medium i. ε_i is the

dielectric constant of the ith medium. Subscripts 1, 2, and 3 refer to the guiding layer, metal layer (coupling layer and substrate), and air, respectively. $k_0 = 2\pi/\lambda$ is the wavenumber in vacuum. $\beta = k_0(\varepsilon_i)^{1/2}\sin\theta$ is the propagation constant of the guided mode.

By using the weak-coupling condition, $\exp(-2p_2h) \ll 1$, the reflection coefficient near resonance can be approximated as [15]

$$r = e^{-i2\phi_{32}} \times (1 - \{4\,\mathrm{Im}(\beta^0)\,\mathrm{Im}(\Delta\beta^{\mathrm{rad}})\}\{\{\beta - [\mathrm{Re}(\beta^0) + \mathrm{Re}(\Delta\beta^{\mathrm{rad}})]\}^2 + \{\mathrm{Im}(\beta^0) + \mathrm{Im}(\Delta\beta^{\mathrm{rad}})\}^2\}^{-1})$$
(3)

where β^0 is the propagation constant of a guided mode for a three-layer waveguide in which the thickness of the upper metal layer is semi-infinite. The imaginary part of β^0, $\mathrm{Im}(\beta^0)$, called intrinsic damping, represents an absorption loss of the guided wave. $\Delta\beta^{\mathrm{rad}}$ represents a difference of eigen-propagation constant between the three-layer waveguide and the free space coupling system. The imaginary part of $\Delta\beta^{\mathrm{rad}}$, $\mathrm{Im}(\Delta\beta^{\mathrm{rad}})$, is called radiative damping. It represents leakage loss of the guided mode from the SMCW to free space which is inversely proportional to the exponential function, h. $\mathrm{Im}(\Delta\beta^{\mathrm{rad}})$ and $\mathrm{Im}(\beta^0)$ can be approximated as [15]

$$\mathrm{Im}(\beta^0) = \begin{cases} i\varepsilon_{i2}\dfrac{k_0^2\kappa_1^2}{p_2(\kappa_1^2 + p_2^2)\beta d_{\mathrm{eff}}} \\ \quad \text{TE polarization} \\ i\varepsilon_{i2}\dfrac{2p_2^2 + k_0^2\varepsilon_{r2}}{p_2}\dfrac{\varepsilon_1\kappa_1^2}{(\varepsilon_{r2}^2\kappa_1^2 + \varepsilon_1^2 p_2^2)\beta d_{\mathrm{eff}}} \\ \quad \text{TM polarization} \end{cases}$$
(4)

and

$$\mathrm{Im}(\Delta\beta^{\mathrm{rad}}) = \mathrm{Im}\left\{\left[\frac{i\kappa_1}{2\beta d_{\mathrm{eff}}} \times (e^{i2(\kappa_1 d - \phi_{12})} - e^{-i2\phi_{12}})\right]_{\beta=\beta^0} \times e^{-i2\phi_{32}}e^{-2p_2h}\right\}$$
(5)

where ϕ_{12} and ϕ_{32} are determined by equation (2). d_{eff} is the effective thickness of the SMCW, which can be expressed as

$$d_{\mathrm{eff}} = \begin{cases} d + \dfrac{2}{p_2} & \text{TE polarization} \\ d + \dfrac{2\varepsilon_2\varepsilon_1(\kappa_1^2 + p_2^2)}{p_2(\kappa_1^2\varepsilon_2^2 + p_2^2\varepsilon_1^2)} & \text{TM polarization.} \end{cases}$$
(6)

The critical thickness, h_{cr}, for TE and TM polarizations can be determined by setting the intrinsic damping $\mathrm{Im}(\beta^0)$ to be the same as the radiative damping $\mathrm{Im}(\Delta\beta^{\mathrm{rad}})$ in equation (3).

By using the parameters $\varepsilon_1 = 11.6858$ (silicon), $\varepsilon_2 = -28+\mathrm{j}1.8$ (gold), $d = 700\ \mu$m and $\lambda = 859$ nm, the calculated critical thickness h_{cr} for TE and TM polarizations as a function of mode number, i, is shown in figure 2. We can see clearly that the critical thicknesses h_{cr} for TE and TM polarizations differ from each other greatly when the mode number, i, is relatively small, while for ultrahigh order mode, which means the mode number is larger than 1000, the critical thicknesses h_{cr} for TE and TM polarizations are almost the same. The
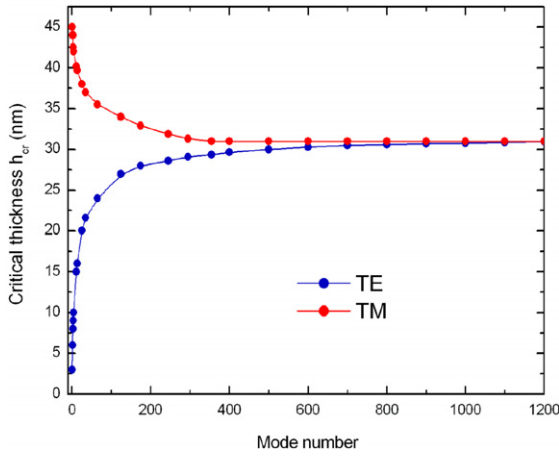
Figure 2. The critical thickness of the upper metal layer, h_{cr}, above which a negative shift is observed and below which, conversely, a positive shift occurs, as a function of mode number for TE and TM polarizations. The parameters are as follows: $\varepsilon 1 = 11.6858$, $\varepsilon_2 = -28 + j1.8$, $d = 700\ \mu m$ and $\lambda = 859$ nm.
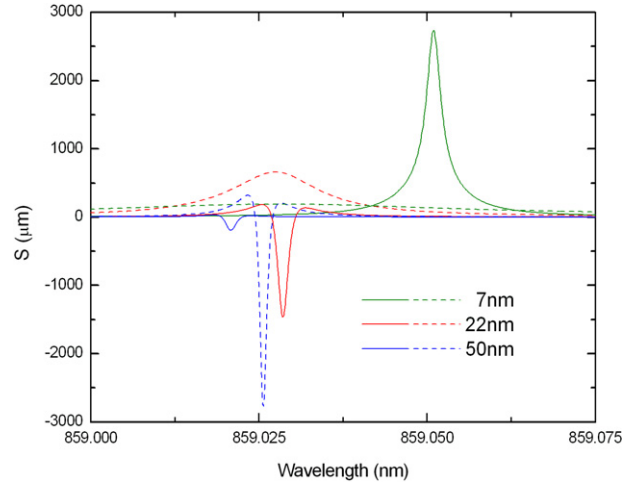
Figure 3. Theoretical calculation of GH shifts for TE (solid line) and TM (dashed line) polarizations versus incident wavelength with various thicknesses of upper metal layer h.

Figure 4. Experimental setup. PD, photodiode; PSD, position-sensitive detector.

explanation is shown as the following. When the incident angle is relatively small, the spectrum of reflected beam is polarization insensitive, which leads to the same GH shifts for TE and TM polarization. Therefore, only when the low order mode is excited can the critical thicknesses h_{cr} for TE and TM polarization be separated from each other.

According to the stationary phase method, the GH shift S is expressed as [16]

$$S(\lambda) = -\frac{\lambda}{2\pi\sqrt{\varepsilon_3}}\frac{d\varphi}{d\theta}\Bigg|_{\theta=\theta_0} \qquad (7)$$

where θ_0 is the fixed incident angle and φ is the phase difference between reflected and incident waves. Figure 3 shows the calculated GH shifts as a function of incident wavelength at various thicknesses h of the upper metal layer for TE and TM polarizations. The incident angle is fixed at 75.27°. The critical thickness, h_{cr}, is 12 nm for TE polarization and 42 nm for TM polarization. For $h > h_{cr}$, negative shift can be observed, while positive shift occurs for $h < h_{cr}$. When the thickness, h, is larger than h_{cr} for TE polarization and less than that for TM polarization, the GH shift obtained under such conditions is negative for TE polarization and positive for TM polarization at the same wavelength. Now, we try to experimentally demonstrate the enhanced and opposite lateral beam shifts in SMCWs.

3. Experiment

The experimental setup for measuring GH shifts is shown in figure 4. For fabricating an SMCW, an upper gold film ($\varepsilon_2 = -28 + j1.8$ at wavelength 860 nm) is sputtered on the surface of a crystal silicon slab ($d = 700\ \mu m$, $\varepsilon_1 = 11.6858$). A 3000 nm thick gold film was sputtered at the back side. The gold film with thickness h and dielectric constant ε_2 was measured by methods introduced by Chen as shown in [17]. The thickness d of the crystal silicon slab was determined by

the m-line technique [18]. After passing through a polarizer, the collimated light beam is incident on the upper metal layer of the SMCW. First, we used a photodiode to detect the reflected beam. Then, the operating angle ($\theta = 75.27°$) for maximum GH shift was determined when the reflected light near a certain dip of the spectrum reached the maximum. After the operating angle was fixed, the photodiode was moved out of the light path and the reflected beam was incident into a position-sensitive detector (PSD) directly [19]. The precise wavelength is controlled by a temperature cell.

Figure 5 represents the measured beam shifts S for TE and TM polarizations as a function of wavelength for (a) $h = 22$ nm; (b) $h = 7$ nm; and (c) $h = 50$ nm. For comparison, we also used the stationary phase method to simulate the GH shifts with the same parameters as the experiment. The directions of the measured reflected beam shifts in these three cases are in agreement with the theoretical curves. As shown in figure 5(a), the positive shift for TM polarization can reach 210 μm and the negative shift for TE polarization can reach $-88\ \mu$m with $h = 22$ nm. The difference of
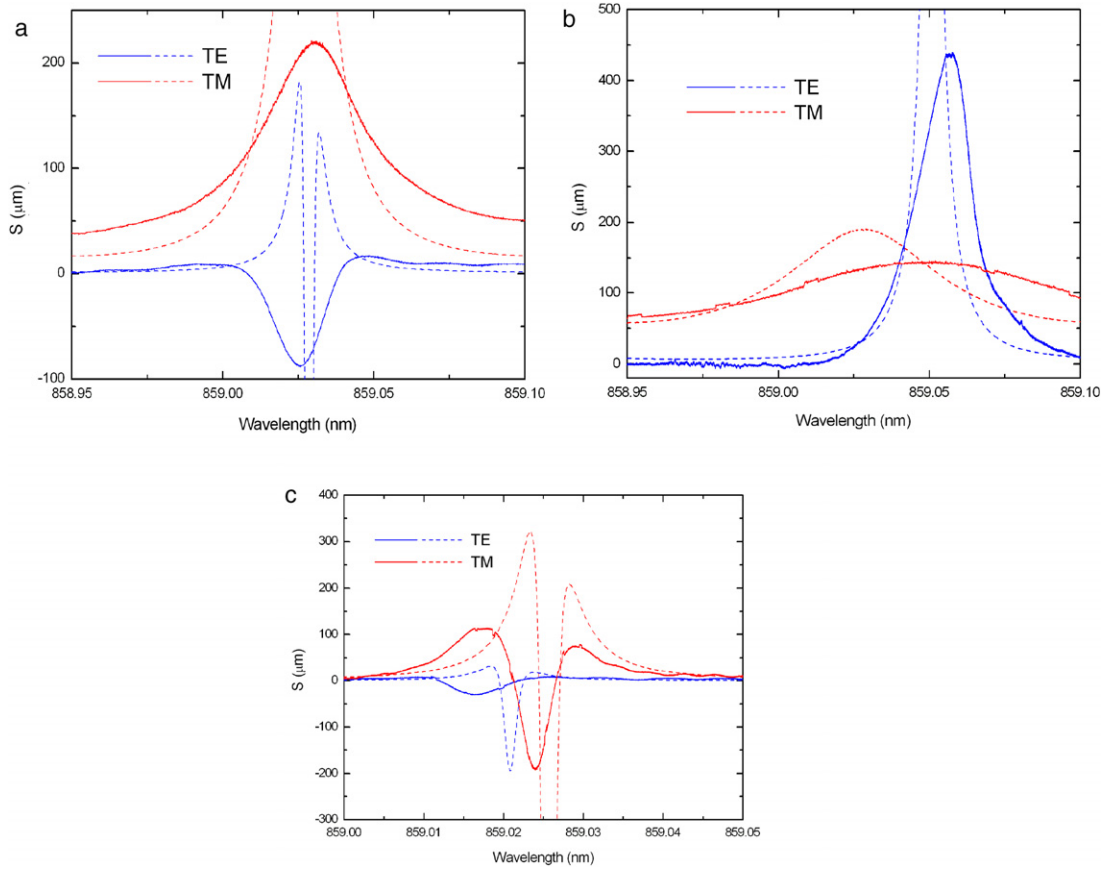
Figure 5. Contrastive graph of experimental results of GH shifts (solid line) *S* together with the theoretical results (dashed line) for TE and TM polarizations versus incident wavelength. The curves have different parameters: (a) $h = 22$ nm; (b) $h = 7$ nm; (c) $h = 50$ nm. The incident angle is 75.27°.

the GH shifts for TE and TM polarization is 260 μm at the wavelength of 859.027 nm. The amplitude of both positive and negative shifts is much larger than that simulated in double-prism structure [8]. In addition, in the experiment the wavelength range that can achieve simultaneous and opposite lateral shift is from 859.005 to 859.045 nm. Within a 40 pm variation of the light wavelength simultaneous and opposite lateral shift can be achieved. Moreover, we calculated that the critical thickness h_{cr} was 12 nm for TE polarization and 42 nm for TM polarization at 75.27° by using equations (4) and (5). Therefore, when the thickness, h, is 22 nm, the GH shift is negative for TE polarization and positive for TM polarization. Furthermore, the profiles of the reflected beams for TE and TM polarizations can be convincingly separated when simultaneously opposite lateral shifts for TE and TM polarizations are excited. This is benefit for the splitting effect, which will be discussed in detail in section 4.

4. Discussion

Actually, the beam shift at the surface of the SMCW has diverged a little, so an incident beam with a finite width has been taken into consideration. We derive here highly accurate expressions for the fields produced by a Gaussian beam incident upon the SMCW and use these results to

examine the reflected fields. Considering an incident beam of Gaussian shape,

$$\psi_i(x, z = 0) = \frac{1}{\sqrt{2\pi}} \int A(\beta) \exp(\mathrm{i}\beta x)\, \mathrm{d}\beta, \qquad (8)$$

the Fourier spectrum of the incident beam $A(\beta)$ is obtained:

$$A(\beta) = w_x \exp[-(w_x^2/2)(\beta - \beta_{x0})^2] \qquad (9)$$

where $w_x = w_0 \sec \theta_0$ and w_0 is the beam width at the waist. The field of the reflected beam is given by

$$\psi_{\mathrm{r}}(x, z = 0) = \frac{1}{\sqrt{2\pi}} \int r(\beta) A(\beta) \exp(\mathrm{i}\beta x)\, \mathrm{d}\beta. \qquad (10)$$

The integration above is extended over the interval $(-k_p, k_p)$, where k_p is the wavevector in the air. The calculated beam shift can be obtained by finding the location where $|\psi_{\mathrm{r}}(x, z = 0)|$ is maximum [3].

To simulate the beam with a finite width, numerical simulations based on the Gaussian model are performed for the reflected TM and TE polarizations with $h = 22$ nm, as shown in figures 6 and 7, respectively. The incident beam waist radius is confined to $w_0 = 200$ μm. For comparison, both the theoretical and experimental results are also shown in figures 6 and 7. The experimental results are in better
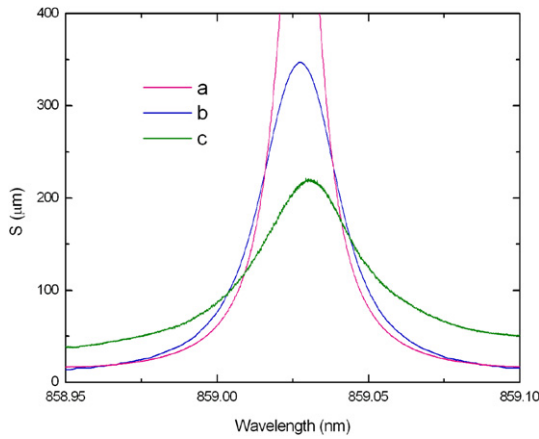
Figure 6. The GH shifts for TM polarization with respect to the incident wavelength at $h = 22$ nm: (a) stationary phase model; (b) Gaussian model with $w_0 = 200$ μm; (c) experimental results.
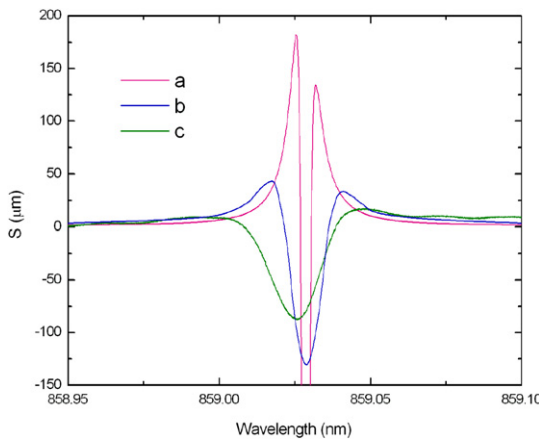
Figure 7. The GH shifts for TE polarization with respect to the incident wavelength at $h = 22$ nm: (a) stationary phase model; (b) Gaussian model with $w_0 = 200$ μm; (c) experimental results.

agreement with the numerical results than the theoretical results. The reason for the large difference between theoretical and numerical curves is as follows. In order to clearly separate the reflected TE beams from TM beams, an incident beam with a narrow finite width is a must, but the narrower the finite width is, the larger the divergence of the light beam is. Large divergence will result in distortion of the reflected beam and deviation of the GH shift, which will be discussed in detail in the following explanations. Furthermore, the maximum beam shifts obtained from experiment are still smaller and the FWHM is broader than the simulated results. This can probably be explained by the nonuniform thickness of the upper metal and nonparallelism of the guiding layer of an SMCW sample [20].

To evaluate the beam splitting effect, we show the pertinent beam profiles for SMCW. Figure 8 shows the measured TE and TM field distributions of the incident beams. The beam shape of the reflected light was detected by a 1/4 inch CCD. For comparison, we simulate a Gaussian shape beam with waist radius 200 μm. We can see that the incident beam profile is of Gaussian shape for TE and TM polarizations. Figure 9 shows the measured reflected TE and
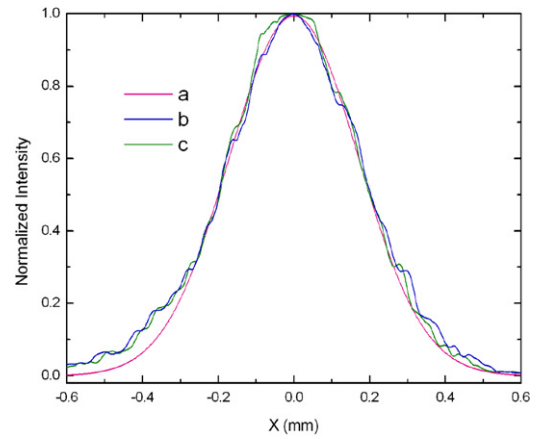
Figure 8. Field distributions of the incident beams on the SMCW surface. The curves have different parameters: (a) simulated profile of Gaussian shape beam with waist radius 200 μm; (b) measured profile of incident TE polarized beam; (c) measured profile of incident TM polarized beam.
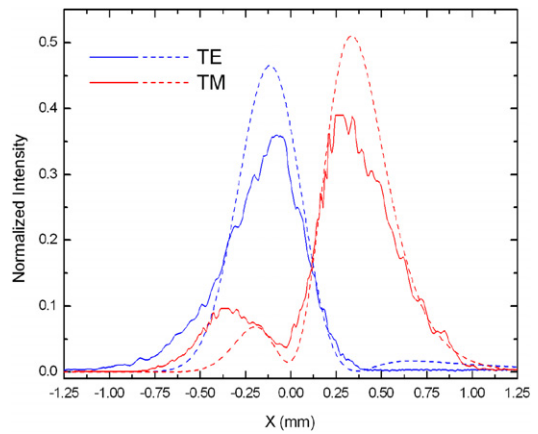
Figure 9. Theoretical (dashed lines) and experimental (solid lines) profiles of the reflected beam for TE and TM polarizations with $h = 22$ nm at incident wavelength 859.031 nm; the incident angle is 75.27°.

TM polarization intensity with $h = 22$ nm at the incident wavelength 859.031 nm. By examining the field produced by a Gaussian beam, we find that the shapes of the reflected beams are different from the Gaussian. This difference is not too great in figure 9. As can been seen from figure 9, the profile of the reflected beam shifts its peak to a different position from the center of the incident beam. The simulated displacement of the reflected beam strongly varies with the light polarization. In our experimental results, as the polarization changes from TE to TM polarizations, the corresponding jump in reflected beam displacement approaches about 0.3 mm. In addition, the normalized maximum reflected intensity of TE (TM) polarization can still reach 0.35 (0.4) experimentally. The splitting effect of the two orthogonally polarized beams coincides with simulated curves.

5. Conclusions

In summary, we report experimentally simultaneously enhanced and opposite lateral shift for TE and TM

polarizations in SMCWs. The critical thickness h_{cr} for TE polarization is much less than that for TM polarization at the low order mode. It is observed that the positive shift for TM polarization can be 210 μm and the negative shift for TE polarization can be -88 μm with the thickness of the upper metal layer 22 nm when the incident angle is 75.27°. Meanwhile, the observed normalized maximum reflected intensity of TE and TM polarization can reach 0.35 and 0.4 at the incident wavelength of 859.031 nm, respectively. Such polarization dependent GH shifts can be applied to optical devices.

Acknowledgments

References

[1] Goos F and Hänchen H 1947 *Ann. Phys., Lpz.* **1** 333
[2] Goos F and Hänchen H 1949 *Ann. Phys., Lpz.* **2** 87
[3] Hsue C W and Tamir T 1985 *J. Opt. Soc. Am.* A **2** 978
[4] Yin X, Hesselink L, Liu Z, Fang N and Zhang Z 2004 *Appl. Phys. Lett.* **85** 372
[5] Pillon F, Gilles H, Girard S and Laroche M 2005 *J. Opt. Soc. Am.* B **22** 1290
[6] Wang L, Chen H and Zhou S 2005 *Opt. Lett.* **30** 2936
[7] Chen L, Cao Z, Ou F, Li H, Shen Q and Qiao H 2007 *Opt. Lett.* **32** 1432
[8] Li C and Wang Q 2004 *Phys. Rev.* E **69** 055601
[9] Hu X, Huang Y and Zhang W 2005 *Opt. Lett.* **30** 899
[10] Wang Y, Cao Z, Yu T, Li H and Shen Q 2008 *Opt. Lett.* **33** 1276
[11] Wang Y, Cao Z, Li H, Jun H, Yu T and Shen Q 2008 *Appl. Phys. Lett.* **93** 091103
[12] Yu T, Li H, Cao Z, Wang Y, Shen Q and He Y 2008 *Opt. Lett.* **33** 1001
[13] Wang Y, Li H, Cao Z, Yu T, Shen Q and He Y 2008 *Appl. Phys. Lett.* **92** 061117
[14] Chen L, Cao Z, Shen Q, Deng X, Ou F and Feng Y 2007 *J. Lightwave Technol.* **25** 539
[15] Cao Z, Qiu L, Shen Q, Dou X and Chen Y 1999 *Chin. Phys. Lett.* **16** 413
[16] Artmann K V 1948 *Ann. Phys., Lpz.* **2** 87
[17] Chen W P and Chen J M 1981 *J. Opt. Soc. Am.* **71** 189
[18] Tien P K, Ulrich R and Martin R J 1969 *Appl. Phys. Lett.* **14** 291
[19] Gilles H, Girard S and Hamel J 2002 *Opt. Lett.* **27** 1421
[20] Raether H 1988 *Surface Plasmons on Smooth and Rough Surfaces and on Grating* (Berlin: Springer)